Aalborg Universitet

Transient delamination growth in GFRP laminates with fibre bridging under variable amplitude loading in G-control

Jensen, S.M.; Bak, B.L.V.; Bender, J.J.; Carreras, L.; Lindgaard, E.

Link to publication from Aalborg University

Citation for published version (APA):
Jensen, S. M., Bak, B. L. V., Bender, J. J., Carreras, L., & Lindgaard, E. (2021). Transient delamination growth in GFRP laminates with fibre bridging under variable amplitude loading in G-control. *Composites Part B: Engineering*, *225*, Article 109296. https://doi.org/10.1016/j.compositesb.2021.109296

Transient delamination growth in GFRP laminates with fibre bridging under variable amplitude loading in G-control

S.M. Jensen *, B.L.V. Bak, J.J. Bender, L. Carreras, E. Lindgaard

The CraCS research group, Dept. of Materials and Production, Aalborg University, Fibigerstraede 16, DK 9220, Aalborg East, Denmark

ARTICLE INFO

ABSTRACT

To predict fatigue-driven delamination growth in real structures, it is inevitable to understand delamination growth under real load spectra, also known as in-service loads, which most commonly are variable amplitude load patterns. In this work, delamination growth in glass fibre-reinforced polymer laminates subjected to two-level block amplitude loading is investigated using a pure moment loaded DCB test configuration for G-controlled cyclic testing. The variable amplitude load patterns consist of single- and periodic repeated load amplitude changes. The method utilises a digital image-based technique that allows for precise tracking of delamination fronts in translucent materials. The work characterises transient crack growth phenomena following load amplitude changes with emphasis on the actual fatigue crack growth rate. The load amplitude changes may increase the crack growth rate by factors of 5–6 in comparison to the crack growth rate in constant amplitude base-line tests. Periodic repeated load amplitude changes particularly increase the fatigue crack growth. For example, after just 10 periodic repeated low- and high-load blocks, the delamination has extended more than a factor of 2 times the delamination extension predicted from a non-interaction model based on constant amplitude data. The effect of the frequency of load amplitude changes on the fatigue crack growth is also investigated. Frequent load amplitude changes are proven to increase the fatigue crack growth significantly because of the transient crack growth responses following the load amplitude changes.

1. Introduction

The majority of fibre-reinforced polymer (FRP) laminated structures undergo cyclic loading of variable amplitude (VA) during operation. The VA load patterns cause a discrepancy between the real fatigue damage accumulation and the damage accumulation as characterised under idealised constant amplitude (CA) loading. The term load interaction effect is commonly used to label the phenomenon that a damage growth increment in a given load cycle depends on the history of load cycles. There are numerous examples in the literature (within fatigue of laminated FRP composites) which demonstrates that VA load spectra cause more damage than CA loading due to load interaction effects. For example the effect of load sequencing [1–6], overload events [7], and frequent changes in load amplitude, also known as cycle-mixing [6,8–12].

Characterisation of load interaction effects in laminated FRP composites is challenging — especially because failure in composites depends on the laminate architecture, and is a result of multiple damage mechanisms (matrix cracking, delamination, fibre fracture, etc.) that sometimes occur independently and sometimes interactively [13]. The conventional damage metrics for analysis of load interaction effects are the number of load cycles to failure or the degradation of macroscopic specimen properties [14] (e.g. the residual strength [2,9] and/or the residual stiffness [6]). However, these damage metrics do not provide information concerning the progression of the underlying mechanisms.

Suitable experimental characterisation techniques have emerged which facilitate to measure the progression of the actual specific damage such as the matrix crack density and the delamination size. For example, the recent automated experimental methods based on digital image processing to measure and track the evolution of matrix cracks [15–17] and the delamination size [18] in glass fibre-reinforced polymer (GFRP) laminates under cyclic loading. This encourages experimental characterisation of the progression of the underlying mechanisms (and their mutual interaction) under VA loading to understand load interaction effects in laminated FRP composites in general [5]. However, few experimental studies are available in the literature in this regard. Considering laminated FRP composites subjected to VA loading, the evolution of intralaminar cracks in fatigue is investigated

in [4,5,17,19,20] and the fatigue crack growth of single macroscopic cracks in [7,21–25].

A few experimental studies are concerned with VA loading and load interaction effects in fatigue-driven delamination growth. This has been investigated using the double cantilever beam (DCB) specimen subjected to displacement-controlled block amplitude loading [7,24, 25]. An increased crack growth due to intermittent overload events are observed in carbon fibre-reinforced polymer (CFRP) laminates in comparison to delamination predictions based on CA data and simple numerical crack growth integration [7]. Load sequence effects are analysed in CFRP laminates [24] and GFRP laminates [25]. The latter study [25] shows a significant transition-behaviour in the crack growth rate following a single step change in load amplitude; the crack growth rate remains different from the response obtained under CA loading at the same applied load level for a significant amount of crack extension [25].

Load interaction effects are most commonly ignored in state-of-the-art delamination prediction models, e.g. crack growth rate models [26, 27]. The models typically evaluate the crack growth rate based on the current cyclic variation of the stress intensity factor or the strain energy release rate (SERR), however, neglect the load history. A sound understanding of load interaction effects in fatigue-driven delamination is essential for developing delamination growth prediction models for variable amplitude loading.

In the remaining of this introduction, G-controlled cyclic testing and basic concepts of large-scale fibre bridging is briefly explained to provide the necessary background before the research questions of this work are presented.

1.1. G-controlled cyclic testing

As the applied VA load pattern increases in complexity, it becomes increasingly difficult to experimentally characterise the crack growth response associated with a given load event. This, among other things, motivates G-controlled cyclic testing and will be elaborated in the current section.

The SERR, G, is often considered as the driving force for crack growth in fatigue. For example, a common practice in characterisation and modelling of fatigue-driven delamination is to assume that the crack growth rate, da/dN, is a function of the cyclic variation of the mode decomposed SERR. This can be represented as $da/dN = f(G_{max}, G_{min}, \phi)$, where G_{max} and G_{min} are the maximum and minimum values of the cyclic varying SERR, respectively, and ϕ is the degree of crack opening mode-mixity [26].

The previous studies of delamination growth in FRP laminates under VA loading [7,24,25] apply the DCB specimen loaded by wedge forces at the crack mouth, e.g. using piano hinges. This follows the ASTM D5528 standard on testing methods to obtain the mode I fracture toughness of UD FRP composites and the ASTM D6115 standard test method for determining the number of cycles for the onset of mode I delamination growth. The same DCB test configuration is often applied for characterisation of the delamination growth rate, e.g. Paris' law relations, in FRP laminates although there are currently no standard test method available for this. The DCB specimen loaded by wedge forces at the crack mouth will be referred to as the standard DCB test configuration in the following.

The standard DCB test is most commonly performed under displacement control or load control. In the standard DCB test, the SERR, G, is continuously changing as the crack propagates, because the SERR, G, is dependent on the crack length regardless of the displacement- or load control mode. The displacement control mode may be preferred for characterisation of fatigue-driven delamination growth because the crack growth rate does not become unstable as the crack length increases, and it is straightforward to initiate the fatigue test from the critical SERR and sweep a large range of G-values. However, the varying SERR, G, with crack extension makes the standard DCB test

inconvenient for G-controlled testing under VA loading and it may obscure the effect of load interactions.

G-controlled cyclic testing can be achieved in different ways. Three different approaches to G-controlled cyclic testing is briefly covered here. The three approaches have been applied in the literature to conduct cyclic testing with constant amplitude and mean value of the SERR, G [28–30], but may be adapted to VA loading in G-control. Cyclic tests in which the amplitude and mean value of the SERR, G, remains constant during the test, will be referred to as constant G-tests in the following.

A constant G-test is proposed in [28] using the displacement-controlled standard DCB specimen with real-time monitoring of the cyclic SERR, G, which is calculated based on compliance measurements and crack length estimations. To obtain constant amplitude and mean values of the SERR, G, the prescribed displacements are adjusted incrementally [28]. Another constant G-test is applied in [29] using a load-controlled width tapered DCB (WTDCB) specimen subjected to wedge forces at the crack mouth. The constant G-test has been applied to investigate mode I cyclic loading of glass/epoxy specimens with fibre bridging [29]. Additionally, the pure moment loaded DCB test configuration has been successfully applied to investigate fatigue crack initiation and propagation in epoxy adhesives under constant G-testing [30].

1.2. Basic concepts in large-scale fibre bridging

Fibre bridging mechanisms are common in the wake of a delamination crack that propagates in FRP laminates. It is well-established that the bridging mechanisms enhance the fracture toughness of an interface [31–33] and reduce the crack growth rate in fatigue [29,34–37]. Cross-over fibre bridging is characterised by a relatively low traction ~ 1 MPa operating over a large crack face separation ~ 1 mm [31–33] (or even larger, for example, 4 mm in UD CFRP laminates [38] and $8 - 10$ mm in UD GFRP laminates [39,40]). This results in a large fibre bridging zone in the wake of the crack tip. The length of the fibre bridging zone is typically comparable to, or larger than, the thickness of the laminate, which is commonly known as large-scale fibre bridging.

Some test specimens are so-called steady-state specimens. In quasi-static loading steady-state specimens ensure steady-state crack growth, that is, when the fibre bridging zone is fully developed, crack growth will occur in a steady-state fashion, in the sense that the fibre bridging zone maintains its size and translates along with the crack tip in a self-similar manner [31,41]. Steady-state specimens are shown to possess several advantages for quasi-static fracture testing when large-scale fibre bridging conditions prevail [31,41]. The steady-state property may also be utilised in fatigue crack growth [41]. In steady-state fatigue crack growth, the crack tip propagates in a self-similar fashion at a constant crack growth rate, and the fully developed fibre bridging zone maintains its size and translates along with the crack tip in a self-similar manner. In such conditions the bridging fibres will undergo identical cyclic opening history, and a constant crack growth rate is feasible [41]. The steady-state situation may be achieved in steady-state specimens with large-scale fibre bridging under constant G-testing. The steady-state property is specially suited to analyse load interaction effects in fatigue-driven delamination growth with large-scale fibre bridging because it enables a suitable base-line steady-state response for comparison of results obtained under VA loading.

The pure moment loaded DCB specimen is a steady-state specimen among the aforementioned constant G-tests in Section 1.1. The pure moment loaded DCB test configuration is well established for quasi-static testing of FRP laminates [38,40,42,43], however, these test fixtures are currently not matured for cyclic testing. Nevertheless, the pure bending moment loaded DCB test configuration has been successfully demonstrated for cyclic testing of epoxy adhesives in [30].
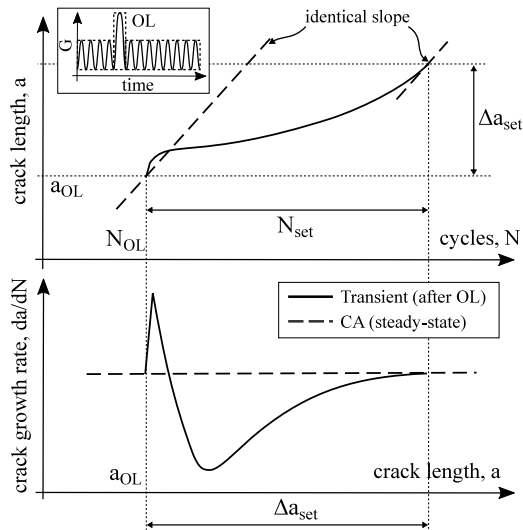
Fig. 1. Schematic example of transient crack growth following an overload (OL) event. Note, after a certain settling crack extension, Δa_{set}, the transient response dies out. *Source:* The figure is based on [44].

(A) A single change in amplitude load level. Left: Low to high (LH). Right: High to low (HL).

(B) Periodic repeated changes in load amplitude level.

(C) Frequent repeated changes in load amplitude level.

Fig. 2. Schematic outline of the load spectra under consideration for research questions (A)–(C).

Fig. 3. Symmetric DCB specimen subjected to pure bending moments M_1 and M_2. Γ_{ext} is a contour integral path along the external boundaries in counter clockwise direction, a represents the crack length, H is the DCB arm height, L is the specimen length, and l_{pz} is the length of the process zone.

1.3. Research questions

The introduction leads to the following research questions on fatigue-driven delamination growth in laminated GFRP composites. The work focuses on characterisation of the transient crack growth following load amplitude changes, as exemplified in Fig. 1. The transient crack growth rate is defined here as any difference in the crack growth rate in comparison to the steady-state crack growth rate obtained in a constant G-test at the same value of SERR, G. All cyclic tests are conducted in G-control. The term CA loading will, therefore, refer to cyclic varying SERR, G, with constant amplitude (and mean) value. The term load amplitude change will refer to an amplitude change in the cyclic SERR, G. The research questions of the current work are divided into the topics (A)–(C) as listed below. Supporting illustrations are provided in Fig. 2.

(A) A single change in load amplitude level: How does a single change in load amplitude, from high (H) to low (L) and from low to high, affect the crack growth rate in comparison to CA loading at the same load levels?

(B) Periodic repeated changes in load amplitude level: In the event of multiple load blocks with consecutive changes in load amplitude level, how does the crack growth rate compare with the crack growth rate following a single change in load amplitude level? How is the transient crack growth rate affected by the load history, i.e. previous load cycles and load amplitude changes?

(C) Frequent changes in load amplitude level: What is the influence of frequently periodic repeated changes in load amplitude level, and how does this affect the crack growth rate?

To answer the research questions, two-level block amplitude load spectra are applied to test coupons using a highly capable experimental setup for detecting small crack increments due to the isolated effect of load amplitude changes. Two features of the experimental setup are especially important in this regard. (*I*) A novel test rig for G−controlled cyclic testing utilising the pure moment loaded DCB test configuration. (*II*) A white light digital image-based method for precise monitoring of the delamination front location in translucent materials [18].

The remaining of the paper is organised as follows. Section 2 presents the test rig for G−controlled cyclic testing of pure moment loaded DCB 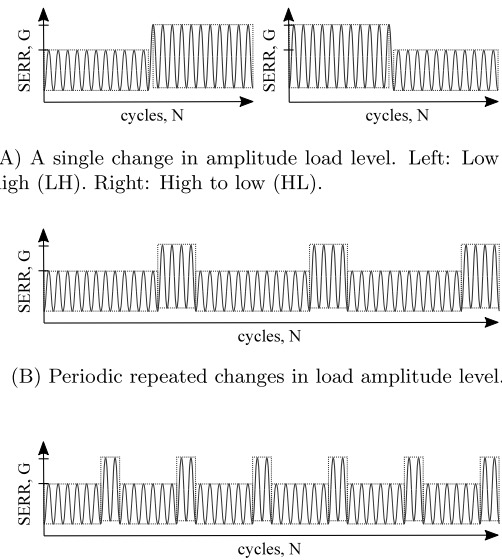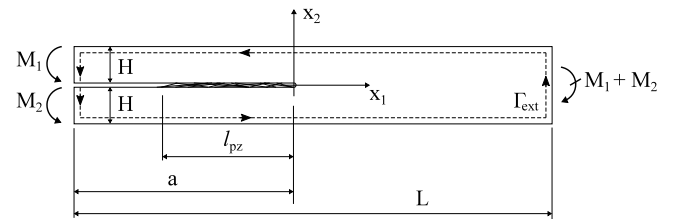specimens with fibre bridging. Section 3 explains the experimental methodology, including a brief description of the digital image-based method for measuring the crack length, the test program, and the fatigue test procedure. The results are presented in Section 4. A discussion of the results are presented in Section 5. Finally, a conclusion is presented in Section 6.

2. Test rig for G−controlled cyclic testing

When delaminations propagate with large-scale fibre bridging, the LEFM solutions (i.e. solutions derived assuming small-scale fracture process zones) of the SERR, G, is flawed, because bridging tractions outside the K-field affect the crack growth [31–33]. Instead, the path independent J-integral can be applied to compute the potential energy release rate accounting for large-scale bridging conditions [45].

2.1. The pure moment loaded DCB specimen

The experimental method is based on a DCB specimen loaded with pure bending moments, as illustrated in Fig. 3. Different crack opening modes can be obtained with this test configuration depending on the values of the bending moments M_1 and M_2. For equal but opposite bending moments, i.e. $M_1 = -M_2$, a pure mode I crack opening mode is obtained and the reaction moment at the right side becomes zero. For pure mode II the bending moments are equal, i.e. $M_1 = M_2$. Mixed-mode crack opening occurs when the bending moments M_1 and M_2 are of different size.

To compute the SERR, G, the J-integral is evaluated along the contour integral path Γ_{ext} in Fig. 3. For an orthotropic laminate under plane stress conditions, the J-integral can be computed as follows [42, 46,47]:

$$G = J = \frac{21(M_1^2 + M_2^2) - 6M_1 M_2}{4W^2 H^3 E_1} \quad (1)$$

where E_1 is Young's modulus in the longitudinal direction of the specimen, W is the specimen width, and H is the height of the DCB arms. For pure mode I crack opening, i.e. $M_1 = -M_2 = M$, the J-integral can be computed as:

$$G = J = \frac{12M^2}{W^2 H^3 E_1} \quad (2)$$

Note from Eqs. (1) and (2) that the SERR, G, is independent of the crack length, a, and does not depend on details of the process zone (process zone size, l_{pz}, bridging law, etc.). Additionally, the SERR is directly proportional to the squared value of the applied bending moment, M, which allows for direct control of the governing fracture parameter, $G(M)$, by simply controlling the applied bending moment.

The pure moment loaded DCB test configuration is convenient for analysis of fatigue-driven delamination under VA loading for several arguments as summarised here, which are not applicable in the standard force- or displacement-controlled DCB test. (I) The isolated effect of VA loading becomes clear as the crack growth driving force (G) does not depend on the crack length. (II) The test configuration provides a simple and accurate evaluation of the SERR, G, in Eq. (2) for small- and large-scale fracture process zones. (III) The steady-state property, see Section 1.2, of the pure moment loaded DCB specimen is convenient to analyse the transient crack growth rate due to load amplitude changes. (IV) Finally, according to Paris' law-like relations there is a direct relation between the cyclic variation of the SERR, G, and the crack growth rate, da/dN, thus keeping the amplitude and mean value of the cyclic bending moment, M, constant gives a constant crack growth rate throughout the test.

2.2. Practical implementation

The current test rig is a further development of an existing test rig, which has been developed in [40,43] for quasi-static testing of DCB specimens subjected to uneven bending moments capable of mode-mixities ranging from pure mode I loading to pure mode II loading. The test rig is enhanced to be able to conduct cyclic testing of DCB specimens under mode I loading. An image of the full test rig is shown Fig. 18 in Appendix and a zoom-in of the DCB specimen and the local load introduction is shown in Fig. 4.

The pure moment loading of the DCB specimen is achieved through a rope and pulley system. The load is introduced from a linear actuated piston of a servo-hydraulic test machine and distributed into the test rig by a Dynema rope. The rope is lead through a system of rope-guide rollers with low friction ceramic bearings. From the rope system, the load is transferred into two moment arms, see items no. 2 in Fig. 4. The moment arms are directly attached to the tabs on the DCB specimen, and are oriented parallel with respect to the DCB specimen's longitudinal direction. Ultimately, the force applied by the piston is converted into a force couple acting on each moment arm, which introduces the bending moments to the DCB specimen. Previous kinematic and experimental studies of the test rig reveal almost perfect introduction of pure bending moments into the DCB specimen with negligible introduction of spurious normal and shear forces [40,43]. The reader is referred to [40,43] for more information on the general operating principle of the test rig.

Strain gauges SG-A to SG-D cf. Fig. 4 are mounted in gauge sections on the moment arms near the load introduction to the DCB specimen. The strain gauges are mounted on the upper and lower surface of each moment arm and provide local measurements of the applied bending
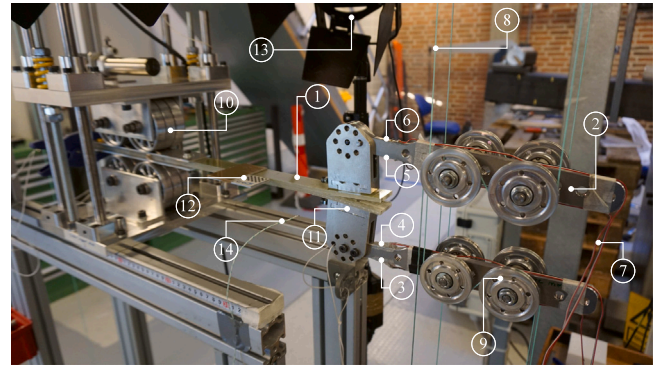

Fig. 4. Annotations: 1: DCB specimen. 2: Moment arm. 3-6: Strain gauges SG-A, SG-B, SG-C, SG-D, respectively. 7: Strain gauge cables. 8: Rope. 9: Rope guide rollers. 10: Specimen support structure. 11: Specimen tabs. 12: Checkerboard. 13: Lights. 14: Type K thermocouple. An image of the full moment rig is included in Appendix.
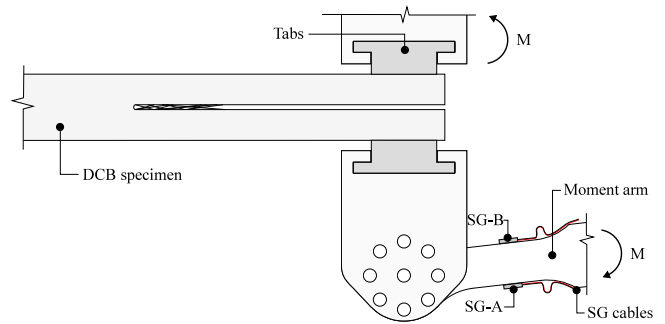

Fig. 5. Schematic outline of the moment transducer installed on the lower moment arm. SG cables are connected to the controller of the test machine.

moment, M. At the lower moment arm, two $120\,\Omega$ active strain gauges, i.e. SG-A and SG-B in Fig. 5, are connected in a Wheatstone bridge circuit together with bridge completion resistors inside the controller of the test machine to form a half-bridge. The half-bridge measures the bending strains and compensates for temperature effects. The strain gauge half-bridge on the lower moment arm is used as a moment transducer to directly control the applied bending moment, M, throughout the cyclic tests. The moment transducer is calibrated using an Instron 10 kN load cell. Strain gauges SG-C to SG-D on the upper moment arm are used for supplementary monitoring of the resulting moment on the upper moment arm. Additionally, a 10 kN Instron load cell is installed to measure the rope force during the tests.

The bending moment will be prescribed according to two-level block amplitude load spectra, which involves step changes in load amplitude. An example showing the actual applied maximum moment, M_{max}, during a step change of the moment amplitude target signal in a 2.5 Hz cyclic test is shown in Fig. 6(a). The response of the moment transducer (SG-A and SG-B) is compared to the supplementary moment measurements from SG-C and SG-D (on the upper moment arm). The responses are consistent and approach the target value from below at the low to high (LH) and high to low (HL) step changes. The relative error in the maximum applied moment in comparison to the target signal are shown in Fig. 6(b) for the LH- and HL step changes. After a cycle increment of $\Delta N = 20$ load cycles, the responses are approximately -5% from the target value, and at $\Delta N = 40$ load cycles a relative error of -2% is observed. This should be kept in mind when transient crack growth responses following load amplitude step changes are analysed in the following.
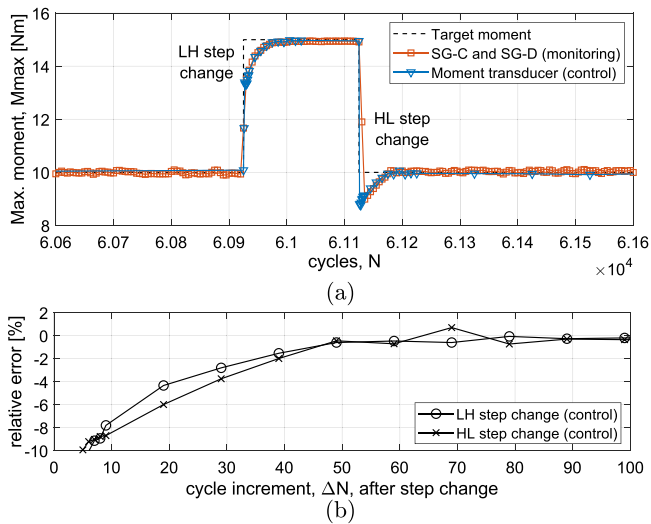
(a)

(b)

Fig. 6. (a) Maximum applied moment during an amplitude step change in a cyclic test at 2.5 Hz. (b) The relative error of the moment transducer in comparison to the target signal after the LH- and HL-amplitude step changes.

3. Experimental methodology

3.1. Materials and test specimen

The laminates consist of 16 plies non-crimp UD (0°) glass fibre mats with an areal weight of 700 g/m². The fibre mats have approximately 8 wt% backing fibres at ±80° and approximately 2 wt% stitching, which keeps the backing fibres attached to the 0° fibres. The laminate is symmetric with respect to the crack plane $(x_1 x_3)$ and the $x_1 x_2$-plane, cf. Fig. 3. The fibre mat lay-up ensures that a pure UD (0°/0°) interface exists at the crack plane, i.e. no backing fibres in the crack plane. An artificial pre-crack is introduced in the laminate mid-plane by a 13 μm thick poly-tetrafluoroethylene (PTFE) film. The laminates are manufactured through vacuum assisted resin transfer moulding using a standard infusion epoxy (PRO-SET INF-114, INF-213) according to the manufacturer's schedules for curing and post-curing. Test specimens are machined into the following nominal dimensions using a diamond saw blade: Specimen length $L = 540$ mm, width $W = 30$ mm, laminate thickness $2H = 8.7$ mm, artificial pre-crack length $a_0 = 50$ mm.

The crack propagates in a 0°/0° ply interface with considerable fibre bridging in the crack wake. The rising fracture resistance under quasi-static crack propagation is reported in Fig. 7 for the current material system. The R-curve is measured using the pure moment loaded DCB test configuration as illustrated in Fig. 3. The R-curve is expressed in terms of the applied bending moment, M, and the crack extension, Δa. Notice from Eq. (2) that the SERR, G, is directly proportional to the squared value of the applied bending moment, $G \propto M^2$. Prior to the R-curve measurement, a natural pre-crack is generated by 3 mm quasi-static propagation of the crack. The crack extension is measured using the method presented in Section 3.2. The R-curve reaches a plateau level, M_{ss}, at a crack extension of $\Delta a = 40$ mm. An average value of the applied bending moment is computed in the interval $\Delta a = [40; 78]$ mm, which gives a plateau value of $M_{ss} = 23.58$ N m.

3.2. Automated measuring of the delamination front

The crack length is measured using a camera, which is attached to the frame structure of the test rig as shown in Fig. 18 in Appendix, and a digital image-based method for automated tracking of the delamination front locations in translucent materials, which has been developed in a previous work [18].
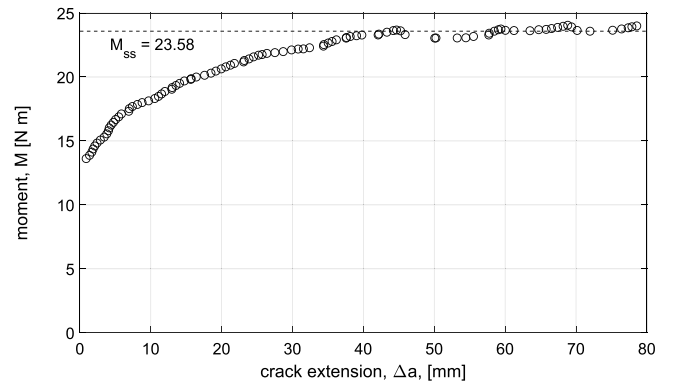

Fig. 7. R-curve expressed in terms of the applied bending moment, M, and the crack extension Δa. Notice from Eq. (2) that $G \propto M^2$.

The basic hardware behind the method is a monochrome FLIR Blackfly CCD type camera with a resolution of 2448 x 2048 pixels, two cool LED white light sources NILA Zaila Daylight to illuminate the DCB specimen, and a computer for image acquisition and storage. The computer counts the number of load cycles in real-time and triggers the camera to acquire an image at predefined load cycle increments ΔN_{IM}, which determines the temporal resolution of the crack length measurements. The process is fully automated and continuous without interrupting the cyclic test.

The basic principle behind the method is the correlation between the crack front and the diffuse reflected light in translucent materials, i.e. glass-epoxy laminates. The crack face separation and irregular surface of newly formed crack area causes an increased intensity of diffuse reflected light in the very early stages of damage, such that damaged and undamaged regions of the specimen can be visually identified.

The camera records the DCB specimen from above as illustrated in Fig. 8(a) with a field of view (FOV) as shown in Fig. 8(b). The FOV includes the region of interest (ROI) and a reference pattern also known as a checkerboard.

The checkerboard is co-planar with the top surface of the undamaged part of the specimen. The checkerboard is the basis for mm/pixel scaling and a 2D projective geometric transformation, which is applied to every acquired image. The transformed image is translated to an exact user-specified location, and the transformed image coordinate system is orientated such that the image plane appears to be perpendicular to the camera viewing direction. The transformation implies that the actual camera viewing direction does not necessarily need to be perpendicular to the specimen top surface and compensates for any movement of the specimen and/or camera during the test. The transformed image has a constant and known pixel/mm scaling on the specimen top surface such that it can be used for measurements.

The ROI contains a damaged and undamaged region of the specimen as illustrated in Fig. 8(b), where the crack front is the transition between the two regions. A series of image processing operations is applied to the transformed image in order to identify the crack front across the specimen width, as indicated by the red curve in Fig. 8(c). Notice that the crack front is thumbnail shaped due to anticlastic bending effects, and the crack length, a, is the average crack length across the specimen width as illustrated in Fig. 8(a). Additionally, the diffuse reflected light occurs in the very early stages of damage [18], thus the measured crack length is the distance to the crack tip as indicated by, a, in Fig. 3, and not the end of the fracture process zone (i.e. $(a - l_{pz})$).

The crack tracking method outputs the crack length, a, as a function of the number of load cycles, N. The noise level on the average crack length across the specimen width is on the order of 0.01 mm [18,25]. The crack growth rate, da/dN, is computed for every data point in the
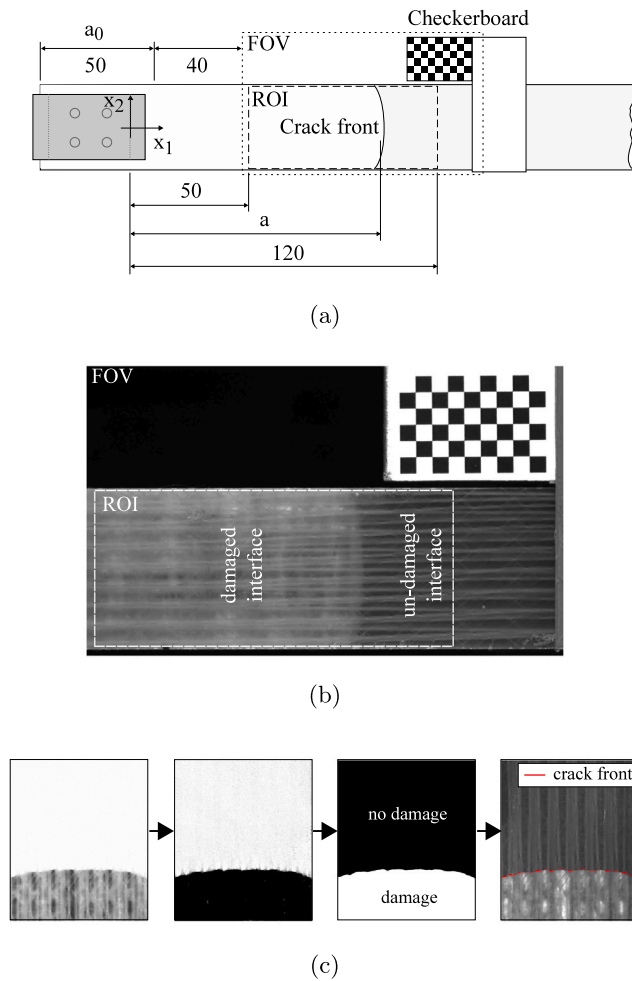
(a)

(b)

(c)

Fig. 8. (a) The DCB specimen seen from above. (b) A sample showing the FOV of the camera. (c) Identification of the crack front (red curve to the right) by application of a series of image processing operations. The reader is referred to [18] for further details.

(N, a)-data set by fitting a linear (polynomial fitting) function to all data points within a moving fitting window, which is centred around the current data point of interest [18].

Finally, the experimental methodology relies on actual crack length measurements as opposed to alternative effective crack length based procedures, e.g. crack length estimates based on measurements of the specimen compliance. The latter procedures are not suited when VA load histories may affect the fracture process zone and hence the specimen compliance.

3.3. Fatigue test procedure

In the following the crack growth rate is measured and analysed in the ROI, which begins at a crack length of $a = 50$ mm, as measured from the tabs cf. Fig. 8(a). Notice in Fig. 8(a) that the crack has to extend 40 mm with respect to the artificial pre-crack, a_0, before reaching the ROI. In the current test procedure, the DCB specimen is subjected to CA loading corresponding to the first load block of the actual cyclic test until the crack length reaches a length of $a = 50$ mm, cf. Fig. 8(a). The test procedure creates a natural pre-crack and a fully developed fracture process zone under the given cyclic loading conditions. This ensures steady-state crack growth, see the definition in Section 1.2, in the beginning of the ROI, and eliminates confounded effects due to the pre-test load history.

The G−controlled cyclic test is realised by directly controlling the applied bending moments, M, as explained in Section 2.2. The applied

bending moments are prescribed according to the two-level block amplitude load spectra as given in Table 1 using sinusoidal waveforms. The applied load patterns are either CA loading or VA load spectra, which consists of CA blocks at two different amplitude and mean values, as illustrated by the load schematics in Table 1. The applied load levels are categorised as either high (H) or low (L), which correspond to a maximum applied bending moment of $M_{max,H} = 15.0$ N m or $M_{max,L} = 10.0$ Nm, respectively. The maximum applied bending moment in the H-load block, $M_{max,H}$, is 64% of the plateau value, M_{ss}, in the quasi-static R-curve in Fig. 7, i.e. $M_{max,H} = 0.64 M_{ss}$. This corresponds to a maximum SERR value in the H-load block, $G_{max,H}$, of approximately $0.64^2 \approx 0.41$ times the plateau value of the fracture toughness in mode I, G_{Ic}^{ss}, because of the relation in Eq. (2), i.e. $G \propto M^2$. The maximum applied bending moment in the L-load block, $M_{max,L}$, is 42% of the plateau value, M_{ss}. This corresponds to a maximum SERR value in the L-load block, $G_{max,L}$, of approximately $0.42^2 \approx 0.18$ times the plateau value of the fracture toughness in mode I, G_{Ic}^{ss}. A load ratio of $R = M_{min}/M_{max} = 0.2$ and a load frequency of $f = 2.5$ Hz is maintained in all tests.

The CA tests at the H- and L-load levels (i.e. CA-H and CA-L, respectively) are used as steady-state base-line measurements to analyse the effect of load amplitude changes in the VA load spectra. The VA-LH and VA-HL tests consist of long load blocks with only a single load amplitude change from one load block to another. These tests are used to study the effect of single load amplitude changes following steady-state crack growth and the effect of load sequencing.

The load spectra in the VA-CM tests include periodic repeated changes in load amplitude to study the effect of such on the transient crack growth following a load amplitude change. The VA-CM tests are further denoted by a number which corresponds to the number of load cycles in the H-load blocks, n_H. The VA-CM tests possess the same ratio of H- to L-load cycles, e.g. $n_H/n_L = 200/20000 = 0.01$, but different load block durations. This increases the number of load amplitude changes by a factor of two in the VA-CM-100 test in comparison to the VA-CM-200 test although the total number of H- and L-load cycles are identical.

The number of repetitions for each load case is given in the second column of Table 1. Two repetitions of the CA loading tests are conducted at each respective load level. Notice that the load history within the first load block of the VA-LH test and VA-HL tests is identical to the CA-L and CA-H tests, respectively (see Table 1). The data from the first load block of the VA-LH and VA-HL tests are therefore considered as CA-L and CA-H data, respectively, such that, the CA data at the L- and H-load levels are made up of three different specimens at each load level. An asterisk symbol (∗) has been added to the repetition number in Table 1 for this reason.

The parameter ΔN_{IM} in Table 1 is the number of load cycles between acquired images. The parameter determines the temporal resolution of the crack length measurements as explained in Section 3.2.

4. Results

Delamination growth caused by the applied load spectra in Table 1 is analysed in terms of the elapsed number of load cycles, N, the average crack length, a, across the specimen width, and the crack growth rate, da/dN. Additionally, the data from VA loading tests are divided into groups depending on the maximum applied load level (H or L) and the elapsed number of H-load blocks, as indicated by the load block numbers in the load schematics in Table 1.

The results section is divided into the following sub-sections based on the research questions in Section 1.3.

- Section 4.1 focuses on the transient crack growth following a single change in load amplitude level. Research question (A), cf. Section 1.3, is the main topic here. Results from CA loading tests are also presented and scatter levels in da/dN-values are estimated. The primary test IDs under consideration, cf. Table 1, are: CA-L, CA-H, VA-LH and VA-HL.

Table 1

Layout of the experimental program. CA-H and CA-L are constant amplitude loading at the H- and L-load level, respectively. VA-LH and VA-HL considers a single load amplitude change in a L to H load sequence and a H to L load sequence, respectively. The VA-CM tests include cycle-mixing with load blocks of different duration.

Test ID	Repetitions	ΔN_{IM}	Load parameters	Load schematic
CA-H High	3*	25	$M_{H,max} = 15.0$ Nm, $R = 0.2$, $f = 2.5$ Hz	
CA-L Low	3*	50	$M_{L,max} = 10.0$ Nm, $R = 0.2$, $f = 2.5$ Hz	
VA-LH Low to High	1	50/20	$M_{H,max} = 15.0$ Nm, $M_{L,max} = 10.0$ Nm, $R = 0.2$, $f = 2.5$ Hz, $\Delta M_{max} = 5.0$ Nm	
VA-HL High to Low	2	20/50	$M_{H,max} = 15.0$ Nm, $M_{L,max} = 10.0$ Nm, $R = 0.2$, $f = 2.5$ Hz, $\Delta M_{max} = 5.0$ Nm	
VA-CM-200 Cycle Mix	1	10/10	$M_{H,max} = 15.0$ Nm, $M_{L,max} = 10.0$ Nm, $R = 0.2$, $f = 2.5$ Hz, $\Delta M_{max} = 5.0$ Nm, $n_L = 20000$, $n_H = 200$	
VA-CM-100 Cycle Mix	2	10/10	$M_{H,max} = 15.0$ Nm, $M_{L,max} = 10.0$ Nm, $R = 0.2$, $f = 2.5$ Hz, $\Delta M_{max} = 5.0$ Nm, $n_L = 10000$, $n_H = 100$	

- Section 4.2 considers multiple load blocks and the effects of periodic repeated changes in load amplitude level. Research question (B), cf. Section 1.3, is the main topic here. The primary test ID under consideration, cf. Table 1, is: VA-CM-200.
- Section 4.3 investigates the influence of cycle mixing by considering load spectra with different load block duration. Research question (C), cf. Section 1.3, is the main topic here. The primary test IDs under consideration, cf. Table 1, are: VA-CM-200 and VA-CM-100.

4.1. A single change in load amplitude level

The crack growth rate during CA loading at the H- and L-load level are reported in Fig. 9 in terms of the crack growth rate, da/dN, as a function of the crack length, a.

The statistical mean, μ, standard deviation, σ, and min–max values are computed for every 2.0 mm of crack extension in the CA-H and CA-L tests. The values are shown in Fig. 9. The average crack growth rate in the CA-H test appears to be constant throughout the test with mean values, μ, in the interval $[3.0;\ 5.0] \cdot 10^{-3}$ mm/cyc and a standard deviation of approximately $2\sigma \approx 2.2 \cdot 10^{-3}$ mm/cyc. The statistical mean over the full crack length range $a = [50;\ 120]$ mm is $\bar{\mu} = 3.6 \cdot 10^{-3}$ mm/cyc. The CA-L tests show a similar response. The average crack growth rate of the CA-L tests appears to be constant throughout the test with mean values in the interval $[0.15;\ 0.30] \cdot 10^{-3}$ mm/cyc, a standard deviation of approximately $2\sigma \approx 0.11 \cdot 10^{-3}$ mm/cyc, and a mean value of $\bar{\mu} = 0.20 \cdot 10^{-3}$ mm/cyc over the full crack length range.

The approximate constant crack growth rate is expected when the cyclic SERR, G, remains constant and the crack propagates under steady-state conditions, cf. Section 1.2. The CA test data are used as base-line in the following to analyse the effect of load amplitude changes on the crack growth rate under CA loading at the same load level.

The effect of a single change in load amplitude is analysed by comparing the crack growth rate in the second load block of the VA-LH test and VA-HL test to the CA-H data and CA-L data, respectively. The crack growth rate is plotted against the crack length in Fig. 10(a) and Fig. 10(b).

The LH load amplitude change occurs (i.e. the H-load block in the VA-LH test starts) at a crack length of $a = 75.4$ mm in Fig. 10(a). An
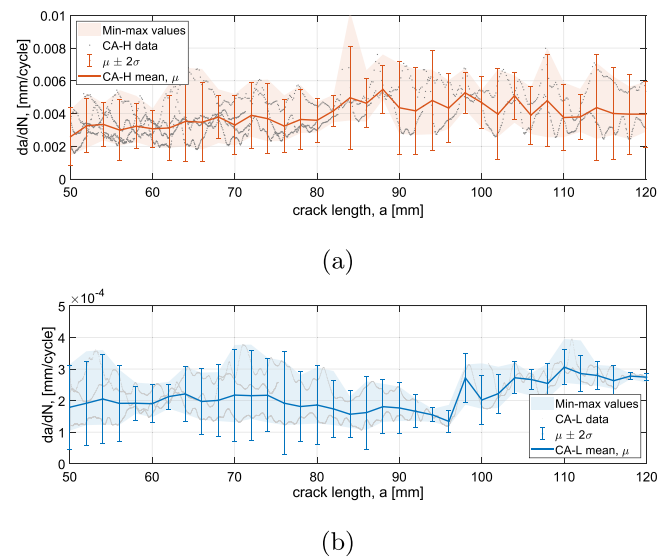
(a)

(b)

Fig. 9. (a) CA-H test data. (b) CA-L test data. The statistical mean, μ, standard deviation, σ, and min–max values are computed for every 2 mm of crack extension. The statistical parameters for the CA-H tests and the CA-L tests are based on approx. 40–80 data points and 300–600 data points for every 2 mm of crack extension, respectively.

increased crack growth rate is measured in the very beginning of the H-load block of the VA-LH test in comparison to the CA-H base-line. The overshoot has a peak value of $da/dN = 17.0 \cdot 10^{-3}$ mm/cyc, which is approximately 4.5 times the statistical mean value, $\bar{\mu}$, of the CA-H test. The crack growth rate in the VA-LH test remains higher than the CA-H test for $\Delta a = 12.6$ mm of crack propagation, however, the overshoot is decreasing as the crack propagates. From $a = 88.0$ mm to $a = 120.0$ mm the crack growth rate is comparable to the CA-H test considering the mean value and estimated standard deviation. Accordingly, the crack growth rate following the LH load amplitude change appears to be a transient overshoot response with a significant settling crack extension, Δa_{set}, cf. Fig. 1.
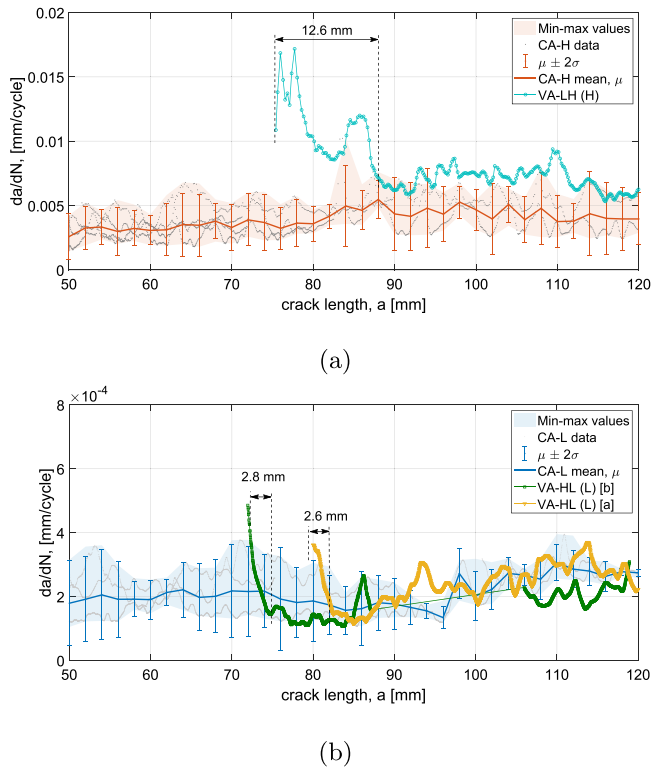
(a)

(b)

Fig. 10. Crack growth rate, da/dN, versus crack length, a. (a) Data from the CA-H test and the H-load block of the VA-LH test. (b) Data from the CA-L test and the L-load block of the VA-HL tests. A short term error in the data acquisition system causes the missing data in the VA-HL [b] test from $a = 88 - 105$ mm.

(a)

(b)

Fig. 11. Crack growth rate versus crack length of the VA-CM-200 test in comparison to CA base-line measurements. The numbers in the graphs refer to the number of elapsed H-load blocks. (a) Crack growth under the L-load level. (b) Crack growth under the H-load level.

The crack growth behaviour following a single load amplitude change in the opposite load sequence is shown in Fig. 10(b). Two VA-HL tests are conducted. The L-load blocks begin at $a = 72.0$ mm and $a = 80.0$ mm in the VA-HL (b) test and the VA-HL (a) test, respectively. The VA-HL tests show a similar tendency. The instant after the HL load amplitude change, the crack growth rate is relatively high in comparison to the CA-L base-line tests. The $(a, da/dN)$-curves exhibit a steep descend during the initial $\Delta a = 2.6 - 2.8$ mm of crack extension. The crack growth rate decreases to approximately $da/dN = 0.12 \cdot 10^{-3}$ mm/cyc, which is within the scatter bands of the CA-L test data. Hereafter, a noticeable change in slope occurs, and the $(a, da/dN)$-curves from the VA-HL tests resembles the CA-L base-line data. No further tendencies in the VA-HL tests can be distinguished from the CA-L base-line test.

4.2. Periodic repeated changes in load amplitude level

The crack growth rate in the VA-CM-200 test is plotted against the crack length in Fig. 11(a) and Fig. 11(b) during the L- and H-load cycles, respectively. Prior to any changes in load amplitude, as indicated by "0" in Fig. 11(a), the crack growth rate conforms well to the crack growth rate in the CA-L tests, as expected. The crack growth rate in the remaining L-load blocks is clearly affected by the presence of the H-load blocks. The crack growth rate in L-load block no. 1 partially resembles the crack growth response observed in the VA-HL tests; a high crack growth rate is measured in the very beginning of the L-load block which is followed by a steep descend. The crack growth rate approaches the CA-L base-line data as the crack continues to propagate. This tendency appears to be repeated throughout the remaining L-load blocks (no. 2–6) in Fig. 11(a).

In Fig. 11(b) a crack growth rate of $14.0 \cdot 10^{-3}$ mm/cyc is measured in the first H-load block (no. 1), which is significantly higher than
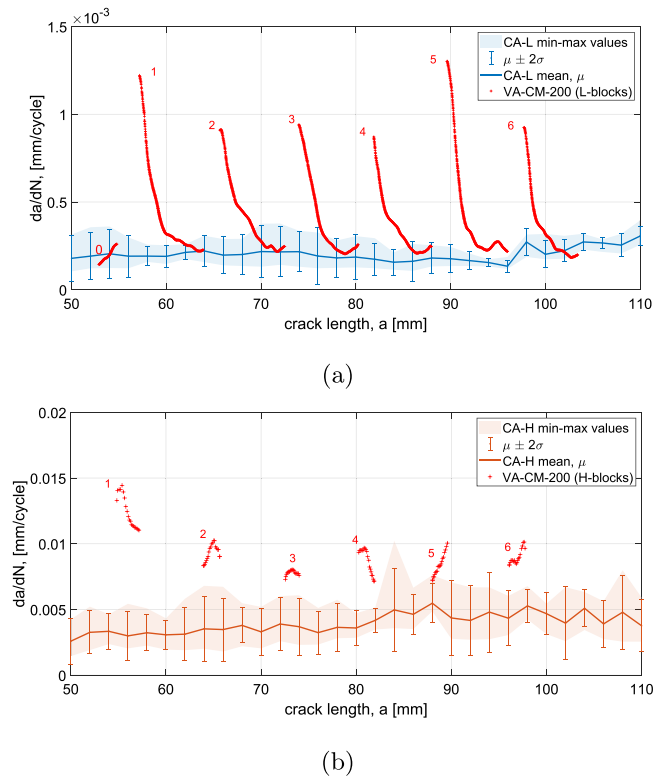
the crack growth rate in the CA-H base-line test. This behaviour is consistent with the transient overshoot response observed in the VA-LH test cf. Fig. 10(a). The crack growth rate in H-load block no. 1 does not settle to the values observed in the CA-H tests during the relatively short duration of the H-load block.

The crack growth rate in the remaining H-load blocks (no. 2–6) reach a peak value of approximately $10.0 \cdot 10^{-3}$ mm/cyc, which is lower than the crack growth rate in H-load block no. 1 and lower than the crack growth rate during the initial H-load cycles in the VA-LH test. Nevertheless, the crack growth rate in all the H-load blocks of the VA-CM-200 test remains higher than the statistical mean values, μ, and scatter bands, 2σ, in the CA-H base-line test.

Results from the VA-CM-200 test may also be analysed across the individual load block numbers as done in Fig. 12. For every H- and L-load block, the crack extension, Δa, and the crack growth rate, da/dN, is plotted against the cycle increment, ΔN. This generates a series of response curves superimposed on top of one another to enable a direct comparison between arbitrary load block numbers. In addition to the VA-CM-200 test results, the crack growth responses following the single change in load amplitude (i.e. the VA-LH and VA-HL tests) are also included in Fig. 12.

The crack extensions during the H-load blocks of the VA-CM-200 test are in the range $\Delta a = [1.5; 2.4]$ mm. The $(\Delta N, \Delta a)$-curves for H-load block numbers 2–6 nearly coincides, while H-load block no. 1 stands out and causes more crack propagation. An equivalent tendency can be seen in Fig. 12(b), which shows a significantly higher crack growth rate in the first H-load block (no. 1) in comparison to the remaining H-load blocks (no. 2–6).

In Fig. 12(a)–(b) a reasonable agreement is observed between the initial 200 H-load cycles of the VA-LH test and H-load block no. 1 of the VA-CM-200 test. The remaining H-load blocks in the VA-CM-200 test
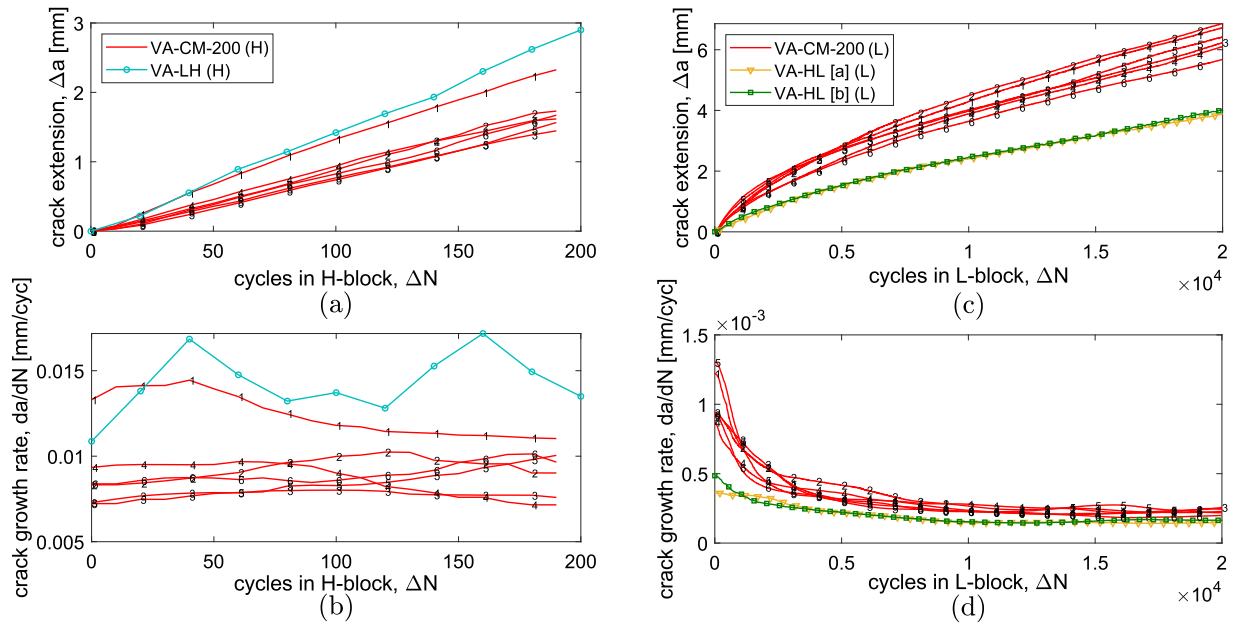
Fig. 12. Crack growth rate, da/dN, and the crack extension, Δa, as a function of the cycle increments, ΔN within the individual load blocks. The marker numbers refer to the load block number. (a) and (b): H-load blocks from the VA-CM-200 test and the VA-LH test. (c) and (d): L-load blocks from the VA-CM-200 test and the VA-HL tests.

(no. 2–6) do not agree with the VA-LH test. This is discussed further in Section 5.1.

The L-load blocks are considered in Fig. 12(c)–(d). The crack extension during the L-load blocks are approximately $\Delta a = 6$ mm, which is 3–4 times the crack extension in the H-load blocks. Consequently, the crack propagates more during the L-load blocks than the H-load blocks for this specific load spectrum.

The $(\Delta N, \Delta a)$-curves for all L-load block numbers show the same tendency. The tendency appears to repeat independent of the load block number, i.e. despite different load histories. Additionally, Fig. 12(d) clearly shows that the crack growth rate is several times higher than the crack growth rate in the base-line CA-L tests ($da/dN \approx 0.20 \cdot 10^{-3} \pm 0.11 \cdot 10^{-3}$ mm/cyc), during a significant portion of the total L-load block duration.

In Fig. 12(c)–(d) the crack extension and crack growth rate during the initial 20000 L-load cycles of the VA-HL tests are compared to the L-load blocks of the VA-CM-200 test. There is a significant difference in the response curves. The crack extension during all L-load blocks of the VA-CM-200 test is larger than the crack extension in the VA-HL tests, and a significantly higher crack growth rate is observed.

4.3. Frequent changes in load amplitude level

The duration of the load blocks in the VA-CM-100 tests is reduced by half in comparison to the load blocks in the VA-CM-200 test. Results from the VA-CM tests, cf. Table 1, are shown in Fig. 13 in the form of load cycles, N, and crack extensions, Δa. The vertical dotted lines indicate time instants where the VA-CM-100 tests and the VA-CM-200 test have experienced an equal amount of L- and H-load cycles. Clearly, more crack propagation occurs in the VA-CM-100 tests compared to the VA-CM-200 test even though the two load spectra have the same ratio between the number of H- and L-load cycles.

In Fig. 14(a)–(d) the crack extension and crack growth rate during the VA-CM tests are plotted as a function of the H-load cycles and the L-load cycles separately. The crack extension and the crack growth rate during the L-load cycles display an obvious difference between the VA-CM-100 and VA-CM-200 tests in Fig. 14(c) and Fig. 14(d). The crack propagates faster in the L-load blocks of the VA-CM-100 test due to the frequent load amplitude changes. The response curves of the VA-CM-100 and VA-CM-200 tests during the H-load cycles, see Fig. 14(a)–(b),
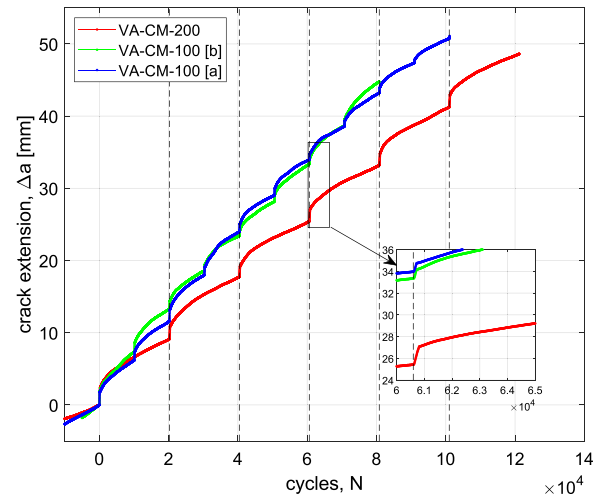

Fig. 13. Number of load cycles, N, versus the crack extension, Δa, in the cycle-mix experiments, VA-CM. Notice, N is counted such that $N = 0$ at the beginning of H-load block no. 1.

are difficult to distinguish. In all the VA-CM tests, the crack growth rate decreases as the number of H-load cycles increases. The response curves in Fig. 14(a)–(b) remain comparable.

The crack growth rate is plotted against the crack length in Fig. 15 for the VA-CM-100 tests in comparison to the CA base-line. The L-load blocks are considered in Fig. 15(a). The two VA-CM-100 tests show the same tendency, which is similar to the results in Fig. 11(a) from the VA-CM-200 test. However, as the duration of the L-load blocks is shortened in the VA-CM-100 tests, the $(a, da/dN)$-curves barely reach a crack growth rate corresponding to the base-line CA-L test before the next H-load block occurs.

The H-load blocks are considered in Fig. 15(b). Generally, the crack growth rate during the H-load blocks are higher than the crack growth rate in the CA-H tests. In H-load block no. 1 of both VA-CM-100 tests, the crack growth rates are within $15.5 - 23.0 \cdot 10^{-3}$ mm/cyc which is approx. 4–5 times the statistical mean value in the CA-H test. The crack
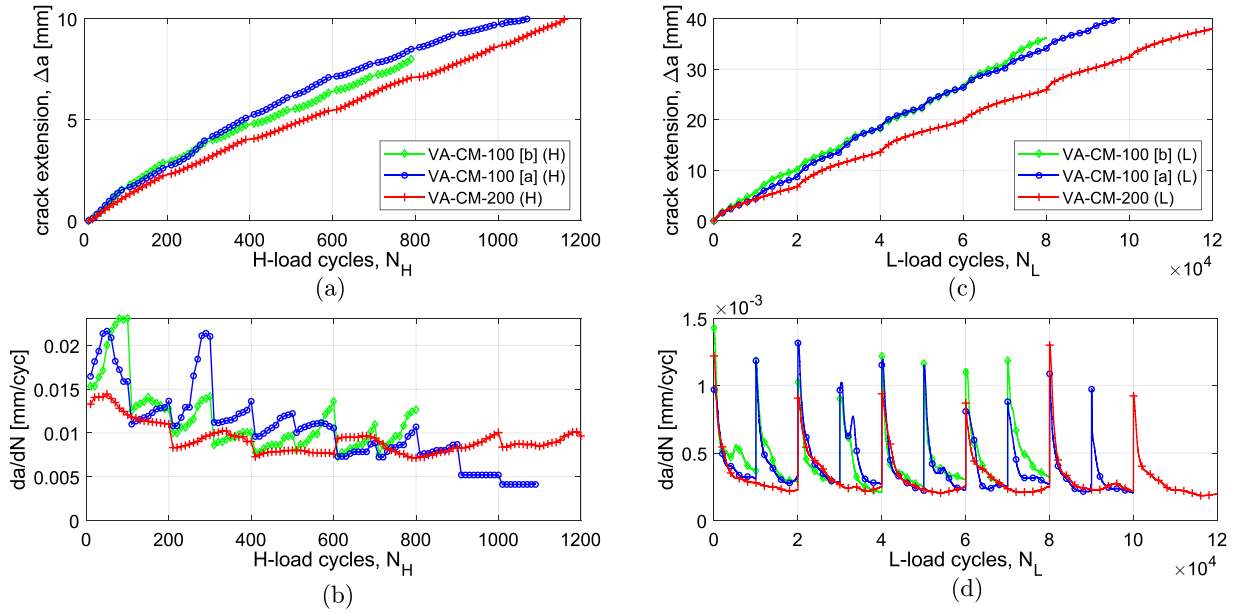
Fig. 14. The VA-CM test data are divided according to the block amplitude load level. (a) Crack extension, Δa, versus the total number of H-load cycles, N_H. (b) Crack growth rate, da/dN, versus the total number of H-load cycles. (c) Crack extension versus the total number of L-load cycles, N_L. (d) Crack growth rate versus the total number of L-load cycles. Note, marker-symbols are only shown for a limited number of data points to visually distinguish the response curves.
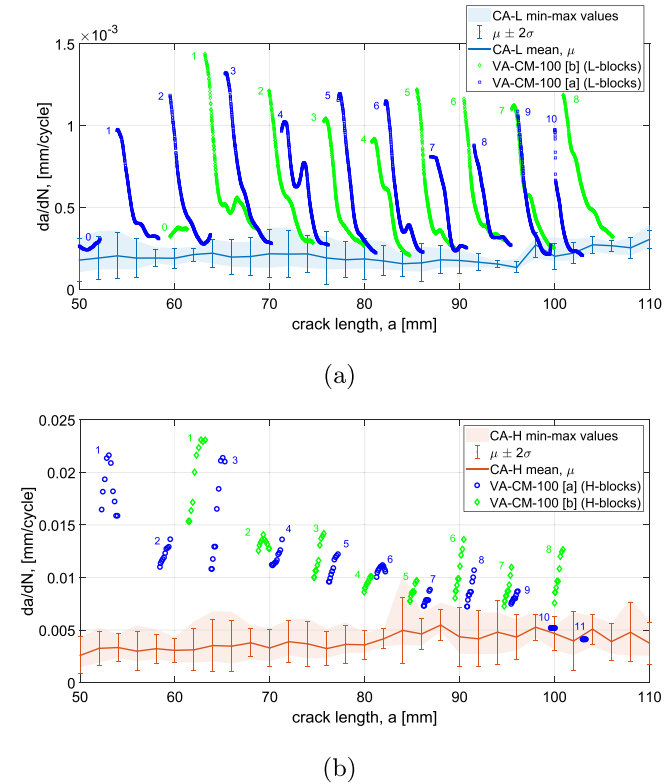

Fig. 15. Crack growth rate, da/dN, versus crack length, a, of the VA-CM-100 tests in comparison to CA loading data at the (a) L-load level and the (b) H-load level.

growth rate during the remaining H-load blocks decreases gradually as the H-load block number increases.

The VA-CM-100 and VA-CM-200 tests are compared in Fig. 16, in which the crack extension and the crack growth rate is plotted against the cycle increment for every H- and L-load block. In Fig. 16(a) and Fig. 16(c) it can be observed that in the VA-CM-100 tests the

crack propagates more during the L-load blocks than during the H-load blocks, which was also the case for the VA-CM-200 test.

Fig. 16(a) shows a gradual decrease in crack extension as the H-load block number increases. The crack extension in H-load blocks no. 1–3 of the VA-CM-100 test decreases in order, while H-load blocks no. 4–8 appear to coincide and conform well to the data from the VA-CM-200 test (except from H-load block no. 1 in the VA-CM-200 test).

The crack extension and crack growth rate during the L-load blocks are shown in Fig. 16(c) and Fig. 16(d), respectively. The responses in the VA-CM-100 test are in good agreement with the VA-CM-200 test. The (ΔN, Δa)-curves and the (ΔN, da/dN)-curves appear to repeat independent of the load block number. Notice in Fig. 16(d) that the L-load blocks of the VA-CM-100 test end around the same time where the (ΔN, da/dN)-curve becomes predominantly constant as opposed to the VA-CM-200 test.

5. Discussion

The discussion is divided into the following sub-sections, which discusses the results according to research questions (A)–(C) in Section 1.3, respectively. The final sub-section briefly discusses the role of bridging fibres during load amplitude changes.

5.1. A single change in load amplitude level

The results in Fig. 10 demonstrates in a simple way that a transient crack growth rate follows a change in load amplitude, which may have an effect on fatigue-driven delamination growth in GFRP laminates. The transient crack growth response in Fig. 10 is a special case with long load blocks of CA cyclic loading, in which the load history is constant prior to the change in load amplitude and the crack propagates under steady-state conditions as defined in Section 1.2. Under these circumstances, the crack growth responses as thoroughly described in Section 4.1 are expected to prevail.

Suppose a single LH load amplitude change is followed by a single HL load amplitude change as illustrated by the three load blocks in Fig. 17. If the number of CA load cycles in L-load block no. 0 and H-load block no. 1 are sufficiently large such that the crack propagates under steady-state conditions prior to the load amplitude changes, then the
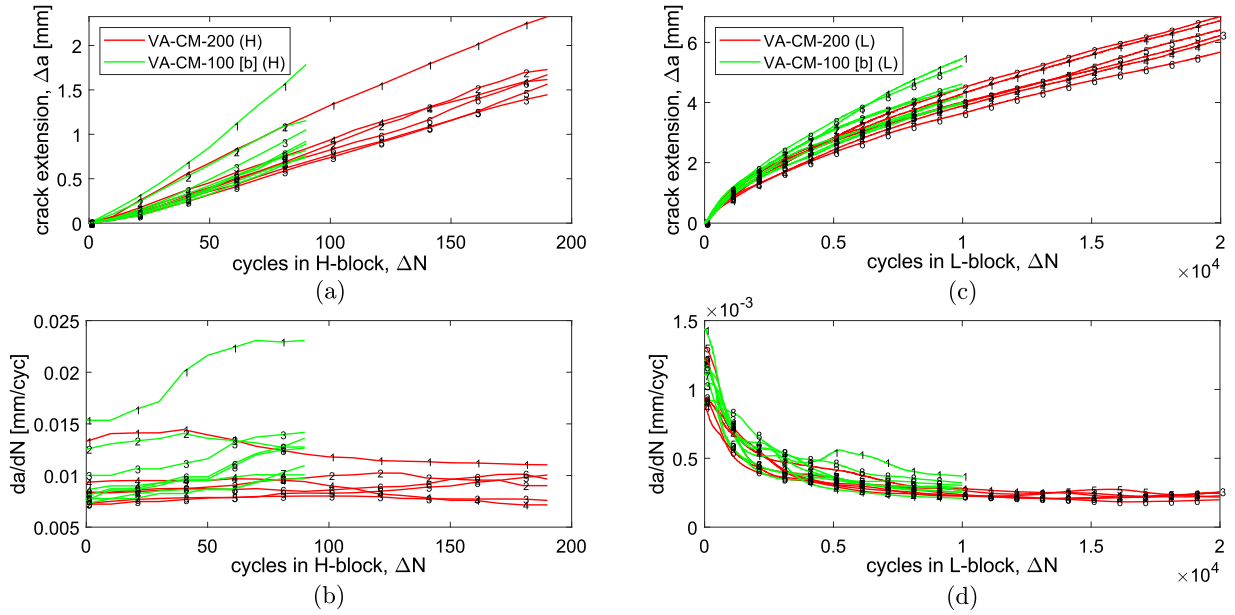
Fig. 16. Analysis of the crack growth rate, da/dN, and the crack extension, Δa, as a function of the cycle increments, ΔN within the individual load blocks. The marker numbers refer to the load block numbers. (a) and (b): H-load blocks from the VA-CM-100 and VA-CM-200 test. (c) and (d): L-load blocks from the VA-CM-100 and VA-CM-200 test.
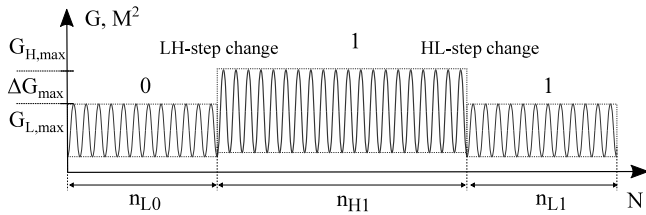

Fig. 17. A two-level block loading spectrum with three load blocks. n corresponds to the number of load cycles within a load block.

response in Fig. 10(a) and Fig. 10(b) is expected to occur at the LH- and HL-load amplitude changes, respectively.

However, if for example the duration of H-load block no. 1, n_{H1} in Fig. 17, is too short to obtain steady-state crack growth before the HL load amplitude change, the transient crack growth response in Fig. 10(b) is not likely to prevail. Instead, it is expected that the crack growth rate is affected to some degree by the VA load history.

The aforementioned example is encountered in H- and L-load block no. 1 in the VA-CM-200 test, cf. Fig. 12. Steady-state crack growth is guaranteed in L-load block no. 0 of the VA-CM-200 test. The load histories in the VA-LH test and the VA-CM-200 test are identical up to the end of H-load block no. 1, which may explain why the response of the VA-LH test is similar to H-load block no. 1 of the VA-CM-200 test in Fig. 12(a)–(b). However, the non-similarity in response curves between L-load block no. 1 of the VA-CM-200 test and the VA-HL tests in Fig. 12(c)–(d) indicates that H-load block no. 1 is too short for steady-state crack growth to occur at the H-load level. This clearly influences the transient response following the HL load amplitude change, the crack grows more in L-load block no. 1 of the VA-CM-200 test in comparison to the initial 20000 L-load cycles of the VA-HL tests.

The example shows that the transient crack growth rate following a single change in load amplitude is neither representative for other load spectra, nor guaranteed to be of conservative nature as the load history may increase the effect of the transient response.

5.2. Periodic repeated changes in load amplitude level

In the following, load interaction effects are discussed when periodic repeated changes in load amplitude level occur. Several noticeable

tendencies in the crack growth rate during the H- and L-load blocks in the VA loading tests are identified in Section 4. The crack growth rate during the H-load blocks of the VA loading test is generally higher than the CA-H base-line test. The crack growth rate in the initial H-load blocks are relatively high, but decreases as the number of H-load cycles increases, see Fig. 14(b). Eventually the crack growth rates in the H-load blocks appear to reach a plateau level, which is higher than the crack growth rate in the CA-H base-line test, but low in comparison to the initial 100–200 H-load cycles of the VA-LH test, cf. Fig. 12(b). Accordingly, the results indicate that the transient crack growth rate following a LH change in load amplitude is likely to reduce in effect when periodic changes in load amplitude level occurs in comparison to the study of a single load amplitude change. Nevertheless, infrequent L-load blocks of long duration may reset the crack growth rate in the transient response to a higher level, due to restoration of steady-state crack growth under the L-load level.

The transient crack growth rates during the L-load blocks of the VA loading tests do not appear to decrease in effect due to periodic repeated changes in load amplitude level. This is indicated in Figs. 12 and 16, where the transient crack growth rate following periodic HL changes in load amplitude appears to repeat independent of the load block number. This indicates that a given H-load block resets the transient crack growth rate in the following L-load block. However, the transient crack growth rate in the L-load block is not identical to the transient crack growth rate following a single HL load amplitude change, i.e. the VA-HL tests, as described in Section 5.1.

5.3. Frequent changes in load amplitude level

To study the effect of frequent load amplitude changes, two load spectra are investigated which possess the same ratio of H- to L-load cycles but different load block durations, as explained in Section 3.3. Recall Fig. 13, which compares the crack extension as a function of the total number of load cycles in the VA-CM tests. A measure of the average load interaction effect for a given load spectrum can be estimated by the ratio between the actual crack extension under VA loading, $\Delta a|_{VA}$, and that predicted by a linear damage accumulation rule (a non-interaction model) using CA base-line data, $\Delta a|_{CA}$. For example, at the right-most vertical dotted line in Fig. 13, $N = 101\,000$, the accumulated number of H-load cycles, $N_H = 1000$, and L-load

cycles, $N_L = 100\,000$, are identical for the VA-CM-100 and VA-CM-200 tests. The crack extension under CA-loading can be estimated by direct summation of crack increments using the CA base-line data in Fig. 9 and the computed average crack growth rates, $\bar{u}$, at each respective load level, see Section 4.1. The resulting estimate neglects load interaction effects. The estimated total crack extension becomes $\Delta a|_{CA} = \Delta a|_{CA-H} + \Delta a|_{CA-L} \approx 23.6$ mm.

The corresponding crack extension in the VA-CM-200 test is $\Delta a|_{VA} = 41.2$ mm at $N = 101000$, cf. Fig. 13, which gives a ratio of $(\Delta a|_{VA}/\Delta a|_{CA}) = 1.75$. A similar exercise is done for the VA-CM-100 test; the crack extension at $N = 101000$ equals $\Delta a|_{VA} = 50.7$ mm, which results in a ratio of $(\Delta a|_{VA}/\Delta a|_{CA}) = 2.15$.

This clearly proves that frequent changes in load amplitude increases the crack extension, and exemplifies the severity of neglecting load interaction effects since this would produce critically non-conservative predictions of fatigue-driven delamination growth.

The reason why frequent load amplitude changes are particularly harmful can first and foremost be explained by the response curves in Fig. 15 (and Fig. 11), where the crack growth rates during the H- and L-load blocks in the VA loading test are generally higher in comparison to CA base-line tests. Secondly, comparing the VA-CM-100 and VA-CM-200 tests in Fig. 14 the crack growth responses during the H-load cycles are difficult to distinguish in Fig. 14(a)–(b), but a clear difference is observed during the L-load cycles in Fig. 14(c)–(d). The difference is attributed to the characteristic and repeating transient crack growth response following every HL load amplitude change. Additionally, as the load block duration is decreased, e.g. VA-CM-200 in comparison to VA-CM-100, the transient crack growth rate during the L-load blocks barely reach a level corresponding to the CA base-line test before the next H-load block occurs. This response will repeat in the following L-load blocks.

Ultimately, the VA-CM-100 tests are examples of fatigue-driven delamination growth that is primarily governed by transient crack growth phenomena; there are very few instants where the crack growth rate settles to a steady-state response as obtained under CA loading. The results indicate that this tendency becomes more significant the more frequent that load amplitude changes occur.

5.4. Transient delamination growth and underlying mechanisms

In fatigue-driven delamination growth, the bridging fibres provide a crack tip shielding effect, which is sometimes expressed as [35,37]: $G_{tot} = G_{tip} + G_{fpz}$, where G_{tot} is the total external SERR, G_{tip} is the actual SERR experienced at the crack tip, and G_{fbz} represents a crack tip shielding effect exerted by the fibre bridging zone (FBZ). It is the authors' opinion that the transient delamination growth following load amplitude changes can be explained by the behaviour of the FBZ and its interaction with the macroscopic crack tip.

A few hypotheses on the role of fibre bridging during load amplitude changes have been suggested in the literature to explain load sequence effects [21,23–25]. The hypotheses have not been validated against experimental observations and/or micromechanical models, and there is yet no consensus on the actual behaviour of the FBZ. A discussion on the different hypotheses in the literature may be found in a previous publication by the authors [25]. One hypothesis concerns a history- and load level dependency on the amount of bridging fibres in the crack wake [25]. The hypothesis suggests that the higher the applied load level, the higher amount of bridging fibres develop in the crack wake. This is a hypothetical corollary of the origin of fibre bridging, which, aside from nesting during laminate manufacturing [48], has been suggested to be partly attributed to a crack tip plastic zone that extends beyond several plies of the delamination plane in tough resin matrices [48,49]. The hypothesis from [25] may explain the increased crack growth rate following the LH load amplitude change, e.g. Fig. 10(a), because of an under-developed FBZ in the VA test immediately after the LH load amplitude change in comparison to the

CA-H baseline test. However, the hypothesis in [25] is inadequate to explain the observed transient delamination growth following the HL load amplitude changes in the current work.

Additionally, the authors in Ref. [25] performed a microscopy inspection of the FBZ in DCB specimens fatigue tested at different load levels with/without single load amplitude changes using the standard DCB test. The authors investigated the FBZs for differences in FBZ configurations and excessive fibre breakage due to load amplitude changes, however, the results were inconclusive [25]. To confirm/reject hypotheses and physically explain the behaviour of the FBZ during load amplitude changes, the authors believe that it requires further studies involving joint experimental observations, e.g. microscopy and/or SEM of the FBZ in specially designed DCB specimens, and micromechanical models of the bridging fibre phenomenon. It is also relevant to look into other damage mechanisms than the FBZ. For example, the effect of intermittent overload events on the fatigue crack extension in carbon/epoxy specimens is investigated in [7]. The authors in [7] suggest that an increased crack extension can be attributed to the formation of an extensive damage zone ahead of the crack tip during the overload events, which decreases the resistance to crack growth in the subsequent L-load cycles.

6. Conclusion

Delamination growth under VA loading is investigated by application of a novel test setup using the pure moment loaded DCB test configuration, which enables G-controlled cyclic testing of fatigue-driven delamination in FRP laminates with large-scale fibre bridging. Steady-state crack growth responses are obtained from constant G-tests, which are used as base-line to analyse the effect of load amplitude changes in two-level block amplitude load spectra. A summary of the answers to the research questions (A)–(C) in Section 1.3 is presented in the following.

(A) A single change in load amplitude level: A single change in load amplitude affects the delamination growth by inciting a transient crack growth response. The transient crack growth depends on the load sequence. A significant increase in the crack growth rate is observed following a LH load amplitude change, which remains higher in comparison to CA-H base-line data for over 12 mm of crack extension. The transient crack growth following a single load amplitude change in the opposite load sequence is less pronounced for the current applied load levels. Immediately after the HL load amplitude change, a relatively high crack growth rate is observed followed by a steep descend in the crack growth rate, which becomes comparable to the CA-L base-line data.

The transient crack growth rate following a single load amplitude change is not a universal response for that particular change in load level nor an extreme case. The load history influences the transient response and may increase the crack growth rate further.

(B) Periodic repeated changes in load amplitude level: Under VA loading with periodic repeated changes in load amplitude level, the crack growth rate is generally higher in comparison to CA base-line tests.

The transient crack growth rate during consecutive H-load blocks is not necessarily a repeated response. A higher crack growth rate is observed in the initial H-load blocks in comparison to later H-load blocks. The crack growth rate during all H-load blocks in the VA loading test remains significantly higher than the CA-H base-line test. However, the crack growth rate in the H-load blocks is generally lower than the peak value in the overshoot response following a single LH load amplitude change.

The crack growth rates during the L-load blocks under VA loading are higher than the CA-L base-line data — particularly in the beginning of the L-load blocks, i.e. immediately after the HL load amplitude changes. The transient crack growth rates are higher than in the studies of a single HL load amplitude change, and continues over a substantial

portion of the L-load block duration. The transient crack growth rates in the L-load blocks appear to repeat independent of the number of elapsed H-load blocks.

(C) Frequent changes in load amplitude level: Frequent load amplitude changes are proved to increase the crack growth rate in comparison to CA base-line data. The reason why frequent load amplitude changes are particularly harmful can be attributed to the transient crack growth rate following the load amplitude changes, which have been identified in the current study. The transient crack growth rate during the VA loading test is several times higher (a factor as much as 4–6) in comparison to CA base-line data. Additionally, the frequent mixing of load blocks prevents the transient response to settle to CA steady-state responses before the next load amplitude change is encountered. This particularly increases the amount of crack extension after a given number of H- and L-load cycles. For example, after a VA load pattern with 10 periodic repeated L- and H-load blocks, the delamination has extended a factor of 2.15 times the delamination extension predicted from CA data and a non-interaction model.

Experiments with frequent load amplitude changes prove that the crack growth responses are predominantly governed by transient responses. The transient crack growth is expected to be equally, or even more, pronounced in many in-service load spectra where frequent changes in load amplitude is common. This further highlights the necessity of taking the transient crack growth into consideration.

In a broader perspective, the results display trends that help to understand general load interaction effects in fatigue-driven delamination growth. The work has characterised transient crack growth phenomena which provide valuable information regarding the progression of the actual delamination growth behaviour. Additionally, the experimental response curves are suitable for benchmarking of future delamination prediction models, e.g. crack growth rate models, which tries to incorporate load interaction effects to avoid dangerous non-conservative life estimations of real composite structures.

CRediT authorship contribution statement

S.M. Jensen: Conceptualization, Methodology, Software, Formal analysis, Investigation, Writing – original draft, Writing – review & editing. **B.L.V. Bak:** Supervision, Conceptualization, Methodology, Software, Writing – review & editing, Funding acquisition. **J.J. Bender:** Software, Resources, Writing – review & editing. **L. Carreras:** Methodology, Resources, Writing – review & editing. **E. Lindgaard:** Supervision, Conceptualization, Methodology, Software, Writing – review & editing, Funding acquisition.

Declaration of competing interest

The authors declare that they have no known competing financial interests or personal relationships that could have appeared to influence the work reported in this paper.

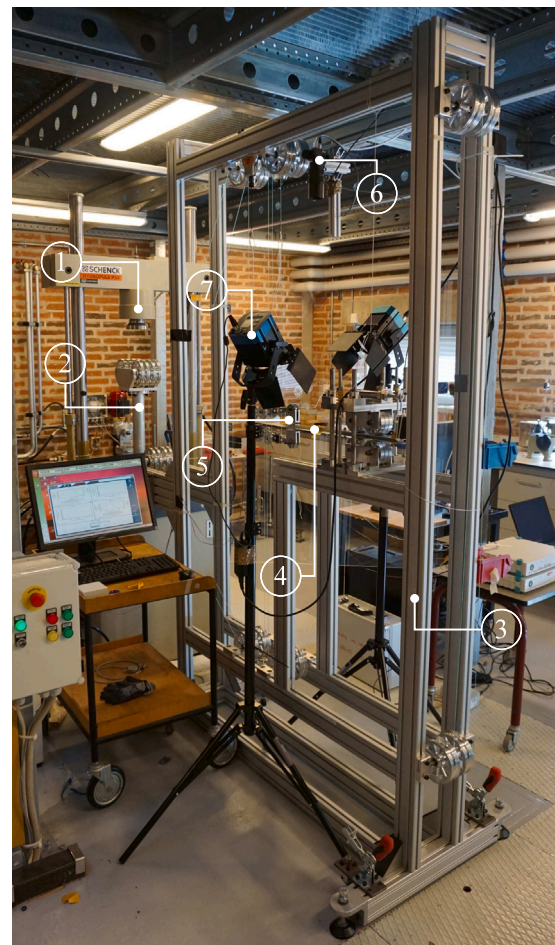## Acknowledgement

Appendix

See Fig. 18.

Fig. 18. 1: Servo-hydraulic test machine. 2: Piston extension piece. 3: Aluminium frame structure. 4: DCB specimen. 5: Moment arm. 6: CCD camera. 7: White light sources.

References

[1] Broutman LJ, Sahu S. A new theory to predict cumulative fatigue damage in fiberglass reinforced plastics. Compos Mater Test Des ASTM STP 1972;497:170–88.

[2] Yang JN, Jones DL. Load sequence effects on the fatigue of unnotched composite materials. Fatigue Fibrous Compos Mater ASTM STP 1981;723:213–32.

[3] Hwang W, Han KS. Cumulative damage models and multi-stress fatigue life prediction. J Compos Mater 1986;20:125–53.

[4] Bartley-Cho J, Lim SG, Hahn HT, Shyprykevich P. Damage accumulation in quasi-isotropic graphite/epoxy laminates under constant-amplitude fatigue and block loading. Compos Sci Technol 1998;58:1535–47.

[5] Gamstedt EK, Sjøgren BA. An experimental investigation of the sequence effect in block amplitude loading of cross-ply composite laminates. Int J Fatigue 2002;24:437–46.

[6] Van Paepegem W, Degrieck J. Effects of load sequence and block loading on the fatigue response of fiber-reinforced composites. Mech Adv Mater Struct 2002;9(1):19–35.

[7] Erpolat S, Ashcroft IA, Crocombe AD, Abdel-Wahab MM. Fatigue crack growth acceleration due to intermittent overstressing in adhesively bonded CFRP joints. Composites A 2004;35:1175–83.

[8] Farrow IR. Damage accumulation and degradation of composite laminates under aircraft service loading: Assessment and prediction, volumes I and II. (Ph.D. thesis), Cranfield Institute of Technology; 1998.

[9] Schaff JR, Davidson BD. Life prediction methodology for composite structures part I - Constant amplitude and two-stress level fatigue. J Compos Mater 1997;31(2):128–57.

[10] Schaff JR, Davidson BD. Life prediction methodology for composite structures part II - spectrum fatigue. J Compos Mater 1997;31 (2):158–81.

[11] Filis PA, Farrow IR, Bond IP. Classical fatigue analysis and load cycle mix-event damage accumulation in fibre reinforced laminates. Int J Fatigue 2004;26:565–73.

[12] Erpolat S, Ashcroft IA, Crocombe AD, Abdel-Wahab MM. A study of adhesively bonded joints subjected to constant and variable amplitude fatigue. Int J Fatigue 2004;26:1189–96.

[13] Degrieck Joris, Van Paepegem Wim. Fatigue damage modeling of fibre-reinforced composite materials: Review. Appl Mech Rev 2001;54(4):279–300.

[14] Hashin Z. Cumulative damage theory for composite materials: Residual life and residual strength methods. Compos Sci Technol 1985;23:1–19.

[15] Glud JA, Dulieu-Barton JM, Thomsen OT, Overgaard LCT. Automated counting of off-axis tunelling cracks using digital image processing. Compos Sci Technol 2016;125:80–9.

[16] Bender JJ, Glud JA, Lindgaard E. Optical high dynamic range acquisition of crack density evolution in cyclic loaded GFRP cross-ply laminates affected by stitching. Composites A 2018;112:207–15.

[17] Bender JJ, Bak BLV, Jensen SM, Lindgaard E. Effect of variable amplitude block loading on intralaminar crack initiation and propagation in multidirectional GFRP laminate. Composites B 2021;217:108905.

[18] Bak BLV, Lindgaard E. A method for automated digital image-based tracking of delamination fronts in translucent glass fibre-laminated composite materials. Strain 2020.

[19] Plumtree A, Melo M, Dahl J. Damage evolution in a $[\pm 45]_{2S}$ CFRP laminate under block loading conditions. Int J Fatigue 2010;32:139–45.

[20] Keiji O, Yashiro S, Niimi K. A probabilistic approach for transverse crack evolution in a composite laminate under variable amplitude cyclic loading. Composites A 2010;41,3:383–90.

[21] Sarfaraz R, Vassilopoulos AP, Keller T. Block loading fatigue of adhesively bonded pultruded GFRP joints. Int J Fatigue 2013;49:40–9.

[22] Sarfaraz R, Vassilopoulos AP, Keller T. Variable amplitude fatigue of adhesively-bonded pultruded GFRP joints. Int J Fatigue 2013;55:22–32.

[23] Vassilopoulos AP. Block and variable amplitude fatigue and fracture behavior of adhesively-bonded composite structural joints. Fatigue and fracture of adhesively-bonded composite joints, Chapt. 9, Elsevier Inc; 2015, p. 257–87.

[24] Yao L, Sun Y, Alderliesten RC, Benedictus R. Fatigue delamination growth behavior in composite materials under block loading. In 31st annual technical conference of the american society for composites: Williamsburg, Virginia, USA, 19-22 September: Vol. 2. 2016. p. 1347–58.

[25] Jensen SM, Bak BLV, Bender JJ, Lindgaard E. Transition-behaviours in fatigue-driven delamination of GFRP laminates following step changes in block amplitude loading. Int J Fatigue 2021;144:106045.

[26] Bak BLV, Sarrado C, Turon A, Costa J. Delamination under fatigue loads in composite laminates: A review on the observed phenomenology and computational methods. Appl Mech Rev 2014;66:1–24.

[27] Turon A, Bak BLV, Lindgaard E, Sarrado C, Lund E. 3 - interface elements for fatigue-driven delaminations in advanced composite materials. In: Hallett Stephen R, editor. Numerical modelling of failure in advanced composite materials. Woodhead publishing series in composites science and engineering, Woodhead Publishing; 2015, p. 73–91.

[28] Manca M, Berggreen C, Carlsson LA. G-control fatigue testing for cyclic crack propagation in composite structures. Eng Fract Mech 2015;149:375–86.

[29] Hwang W, Han KS. Interlaminar fracture behaviour and fiber bridging of glass-epoxy composite under mode I static and cyclic loadings. J Compos Mater 1989;23:396–430.

[30] Dessureault M, Spelt JK. Observations of fatigue crack initiation and propagation in an epoxy adhesive. Int J Adhesion Adhesives 1996;17:183–95.

[31] Suo Z, Bao G, Fan B. Delamination R-curve phenomena due to damage. J Mech Phys Solids 1992;40:1–16.

[32] Bao G, Suo Z. Remarks on crack-bridging concepts. Appl Mech Rev 1992;45, 8:355–66.

[33] Sørensen BF, Jacobsen TK. Crack growth in composites applicability of R-curves and bridging laws. Plast Rubber Compos 2000;29(3):119–33.

[34] Yao L, Alderliesten R, Zhao M, Benedictus R. Bridging effect on mode I fatigue delamination behavior in composite laminates. Composites A 2014;63:103–9.

[35] Donough MJ, Gunnion AJ, Orifici AC, Wang CH. Scaling parameter for fatigue delamination growth in composites under varying load ratios. Compos Sci Technol 2015;120:39–48.

[36] Yao L, Alderliesten R, Benedictus R. The effect of fiber bridging on the Paris relation for mode I fatigue delamination growth in composites. Compos Struct 2016;140:125–35.

[37] Farmand-Ashtiani E, Cugnoni J, Botsis J. Effects of large scale bridging in load controlled fatigue delamination of unidirectional carbon-epoxy specimens. Compos Sci Technol 2016;137:52–9.

[38] Sørensen BF, Jacobsen TK. Large-scale bridging in composites: R-curves and bridging laws. Composites 1998;29A:1443–51.

[39] Jensen SM, Martos MJ, Lindgaard E, Bak BLV. Inverse parameter identification of n-segmented multilinear cohesive laws using parametric finite element modeling. Compos Struct 2019;225:111074.

[40] Lindgaard E, Bak BLV. Experimental characterization of delamination in off-axis gfrp laminates during mode I loading. Compos Struct 2019;220:953–60.

[41] Sørensen BF. Delamination fractures in composite materials. In: A. Talreja, J. Varna, editors. Modeling damage, fatigue and failure of composite materials. Woodhead Publishing Series in Composites Science and Engineering; 2016, Number 65.

[42] Sørensen BF, Jørgensen K, Jacobsen TK, Østergaard RC. Dcb-specimen loaded with uneven bending moments. Int J Fract 2006;141:163–76.

[43] Svenninggaard J, Bak BLV, Andreasen JH, Lindgaard E. Test fixture for double cantilever beam (DCB) specimens subjected to uneven bending moments. In 8th international conference on composites testing and model identification. KU Leuven, 2017.

[44] Skorupa M. Load interaction effects during fatigue crack growth under variable amplitude loading - a literature review. Part I: Empirical trends. Fatigue Fract Eng Mater Struct 1998;21:987–1006.

[45] Rice JR. A path independent integral and the approximate analysis of strain concentrations by notches and cracks. J Appl Mech 1968;35:379.

[46] Suo Z. Delamination specimens for orthotropic materials. J Appl Mech 1990;57:627–734.

[47] Hutchinson JW, Suo Z. Mixed mode cracking in layered materials. Adv Appl Mech 1992;29:63–191.

[48] Johnson WS, Mangalgiri PD. Investigation of fiber bridging in double cantilever beam specimens. Technical Report No. NASA TM-87716, Langley Research Center; 1986.

[49] Bradley WL, Cohen RN. Matrix deformation and fracture in graphite reinforced epoxies. In: Johnson WS, editor. Delamination and debonding of materials ASTM STP 876. Philadelphia: American Society of Testing and Materials; 1985, p. 389–410.